processes

MDPI

Article

Robotic Sequential Ultrasonic Welding of Thermoplastic Composites: From Coupons to a Full-Scale Fuselage Demonstrator

Abhas Choudhary [1,2,*], Ioan Bîrgăoanu-Acăei [2] and Irene Fernandez Villegas [2]

[1] SAM XL Smart Advanced Manufacturing XL, Rotterdamseweg 382c, 2629 HG Delft, The Netherlands
[2] Aerospace Structures and Materials Department, Faculty of Aerospace Engineering, Delft University of Technology, Kluyverweg 1, 2629 HS Delft, The Netherlands; i.birgaoanu-acaei@tudelft.nl (I.B.-A.); i.fernandezvillegas@tudelft.nl (I.F.V.)
* Correspondence: a.choudhary@tudelft.nl

Abstract

Sequential ultrasonic spot welding is an interesting joining method for overlapping thermoplastic composite structures. In the framework of the EU Clean Aviation Multi-functional Fuselage Demonstrator (MFFD) and the lower shell SmarT multifunctional and INteGrated TP fuselage (STUNNING) projects, SAM XL and TU Delft Aerospace Engineering collaboratively developed and demonstrated a robot-based sequential ultrasonic spot welding process for the sub-assembly of structural frames and clips in a fuselage section demonstrator. This full-scale thermoplastic composite fuselage section demonstrator, which was recently awarded the 2025 JEC Innovation award, measures 8.0 m in length and 4.0 m in diameter. Our robot-based sequential ultrasonic spot welding technology played an important role in ensuring the joining of structural clips and frames in the stiffened fuselage skin of the demonstrator, through the use of more than 1600 spot welded joints with an average welding time of approximately 10 s per spot, thereby significantly reducing cycle times as compared to traditional joining methods such as fastening or riveting. This paper provides a comprehensive overview of the technology development process and highlights the results achieved during the sub-assembly of the demonstrator, as well as the challenges encountered.

Keywords: thermoplastic CFRP; ultrasonic welding; spot welding; aerospace structures

Academic Editors: Raul D. S. G. Campilho, Flávia Barbosa and Dan Zhang

Received: 30 November 2025
Revised: 15 January 2026
Accepted: 29 January 2026
Published: 3 February 2026

1. Introduction

In response to the growing need for reducing emissions in the aviation industry, cost reduction, and faster production cycles, there has been a notable push towards the integration of thermoplastic composites into aircraft structures. A prime illustration of this trend is the Multifunctional Fuselage Demonstrator (MFFD) developed under the Clean Sky 2/Clean Aviation Joint Undertaking [1]. This demonstrator highlights a range of technologies that underscore the versatility and cost-effectiveness of thermoplastic composites. Among these technologies are Automated Fiber Placement (AFP), co-consolidation, press forming, Continuous Compression Molding (CCM), injection molding, and thermoplastic welding [2,3]. A key aspect of these techniques lies in harnessing the unique property of the thermoplastic polymer matrix, which enables it to melt when heated and solidify upon cooling. This behavior allows for thermal forming of parts and the possibility of joining using fusion, facilitating the rapid production and integration of structural components.

Ultrasonic welding is a particularly promising joining technology for thermoplastic composites, as it reduces welding times to a couple of seconds per welded spot while offering high joint strength [4,5]. During the welding process, high-frequency, low-amplitude mechanical vibrations are introduced into the composite part by means of a mechanical horn, called a sonotrode. With the help of an energy director (ED), which can be (resin-rich) protrusions molded on the welding surface(s), a neat polymer film, or a mesh, heat generation is mostly focused at the welding interface [6–9]. Heat is generated through frictional heating at the interfaces and viscoelastic heating within the ED and the composite parts [10]. The ED experiences an increased cyclic strain under ultrasonic vibration due to its lower stiffness as compared to the composite part, thus helping focus the heat generation at the interface.

In the past, research has been reported on multi-spot sequential ultrasonic spot welding of thermoplastic composites at the laboratory scale. Here, a discontinuous welded seam was achieved with a table-top welder in a laboratory environment. The welded joint was demonstrated to exhibit comparable load-carrying capability as well as more localized damage upon failure when compared to a mechanically fastened joint of comparable size in a single-lap configuration. This resulted from higher joint stiffness and lower secondary bending, resulting in lower peel stresses in the welded joints [11]. However, some questions that remain unanswered are as follows: what is needed to upscale this technology for the welding of real structures, and to what extent can lessons learned in the research at the laboratory scale be used in this process? Furthermore, the influence of the limited stiffness of industrial robots in high-force contact processes, such as ultrasonic spot welding of structural thermoplastics, has not been characterized. The stiffness of an industrial robot is a complex parameter that changes depending on its posture, the direction of the force, and specific joint angles. Additionally, maintaining precise perpendicular positioning of the weld tooling with respect to the parts being welded, is extremely crucial for weld uniformity. It is not known whether the positioning accuracy and stiffness of industrial robots is sufficient for the welding process. The question remains: can sequential ultrasonic spot welding be up-scaled using industrial robots, and to what extent can the results obtained from a robot-based ultrasonic welding process be compared against a dedicated table-top ultrasonic welding process?

This paper provides answers to the questions above by describing the technology development process undertaken to apply robot-based sequential ultrasonic welding for the sub-assembly of circumferential frames into the stiffened shell of the fuselage demonstrator [12]. In Part I of this paper, a coupon-level study for the development of the welding process is discussed. This included the development of a generic robotic ultrasonic welding end effector (EEF), which was then implemented on an industrial articulated robot for ultrasonic spot welding of coupons. The results obtained from this welding process were compared with those from a commercially available table-top static ultrasonic welder, henceforth known as static welds. Part of the results presented in this part of the paper were reported in our previous work [13]. In Part II, the description of a robot-based welding setup defined for the full-scale demonstrator manufacturing, the challenges faced, and the results obtained are presented. In this part of our work, a specific robotic EEF and two dedicated welding tools were developed to produce ultrasonic spot welds, based on the lessons learned in Part I. Finally, this paper presents the results achieved and the lessons learned from the eventual full-scale demonstrator manufacturing, which will drive further development of this technology.

2. Part I: Coupon-Level Study

2.1. Materials and Methods

2.1.1. Materials, Coupon Manufacturing, and Geometry

Two different thermoplastic composite materials were used in the coupon-level study, including continuous unidirectional carbon fiber-reinforced low-melt polyaryletherketone laminated material (referred to as UD CF/LMPAEK laminates hereafter) and short carbon fiber-reinforced LMPAEK material (referred to as SF CF/LMPAEK material hereafter).

Furthermore, two types of UD CF/LMPAEK laminates were used. The first type was cross-ply UD CF/LMPAEK laminates with a $[0/90]_{3s}$ stacking sequence and a total nominal thickness amounting to 2.16 mm. These cross-ply layup laminates were made from Toray Cetex® TC1225 powder-impregnated tapes and press-consolidated in house using a Joos hot-plate press for 20 min at 370 °C and 10 bar pressure. The second type was quasi-isotropic UD CF/LMPAEK laminates with a stacking sequence of [45/135/90/0/135/45/135/45/45/135/45/135/0/90/135/45] and nominal thickness of 2.88 mm manufactured by Toray Advanced Composites, Nijverdal, The Netherlands. Coupons of sizes 120 mm × 40 mm and 180 mm × 100 mm were cut from these laminates for the welding experiments using a water-cooled circular diamond saw. The coupons were cut with their longitudinal direction parallel to the 0° direction of the laminates. Before welding UD CF/LMPAEK coupons to each other, an energy director was placed in between the adherends. This energy director was a 0.32 mm thick discontinuous LMPAEK film covering the entire overlap area. By discontinuous film, we mean that the energy director consists of a flat film with open areas cut out, as can be seen in the schematic drawings in Figure 1. The energy director film was fixated to the bottom adherend outside of the overlap using Kapton adhesive tape. It should be noted that the fixation of the energy director film was a manual step that was employed for the coupon-level study and may differ from a potential industrial application, where this step could be difficult to automate.

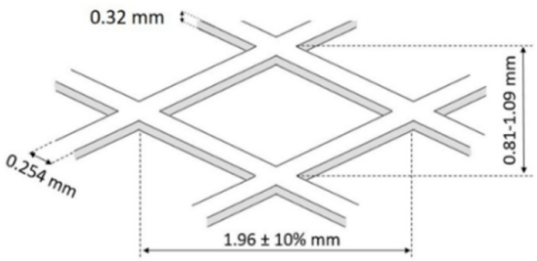

Figure 1. Schematic representation of discontinuous energy director with a thickness of 0.32 mm. Reproduced with permission from [14].

The SF CF/LMPAEK material comprised a commercially available LMPAEK polymer matrix with 40% CF content. The SF CF/LMPAEK coupons had a thickness of approximately 2 mm, and their dimensions were 101.6 mm × 25.4 mm and 150.0 mm × 40.0 mm. They were injection-molded and had 0.2 mm high molded triangular energy director ridges with a 90° apex (see Figure 2). The molded energy director ridges were manufactured at the same time as the coupons by adding a laser-machined insert with a negative microstructure to the injection mold [15]. The dimensions of the molded ED ridges were determined based on previous research, as well as manufacturing constraints to enable one-shot injection molding of the SF CF/LMPAEK material. The coupons were manufactured by AIMEN Technology Centre (Pontevedra, Spain) as part of the ECO-CLIP project. The area covered by the molded energy directors varied for the two types of coupons produced. For the 25.4 mm wide coupons, the ED covered an area of 25.4 mm × 25.4 mm, whereas for the 40.0 mm wide coupons, the ED covered an area of 40.0 mm × 75.0 mm.

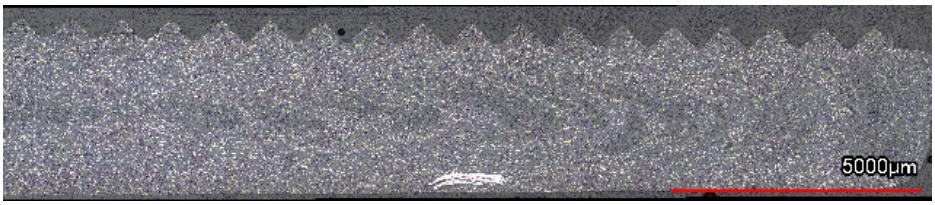

Figure 2. Longitudinal cross-section micrograph of a SF CF/LMPAEK coupon. The triangular ridges molded during panel production (seen on the top of the image) behave as an energy director during welding.

Prior to the welding process, the surfaces to be welded were cleaned with isopropanol to remove grease and other contaminants in the weld interface. Welds were produced in various material configurations during this study. An overview of the welding configurations is provided in Table 1 and Figure 3. It should be noted that in the SF-to-UD welding configurations, the SF CF/LMPAEK material was always the top adherend and the flat surface of the SF CF/LMPAEK adherend was in direct contact with the sonotrode.

Table 1. Overview of welding configurations.

Material Configuration	Weld Type	Overlap Area (mm × mm)	Weld Pattern
UD CF/LMPAEK to UD CF/LMPAEK (cross-ply layup)	Single-spot	40 × 40	One circular spot (Figure 3a)
	Multi-spot	100 × 100	Four circular spots (Figure 3b)
SF CF/LMPAEK to UD CF/LMPAEK (quasi-isotropic layup)	Single-spot	25.4 × 25.4	One circular spot (Figure 3c)
	Two-spot	75 × 40	Two circular spots (Figure 3d)

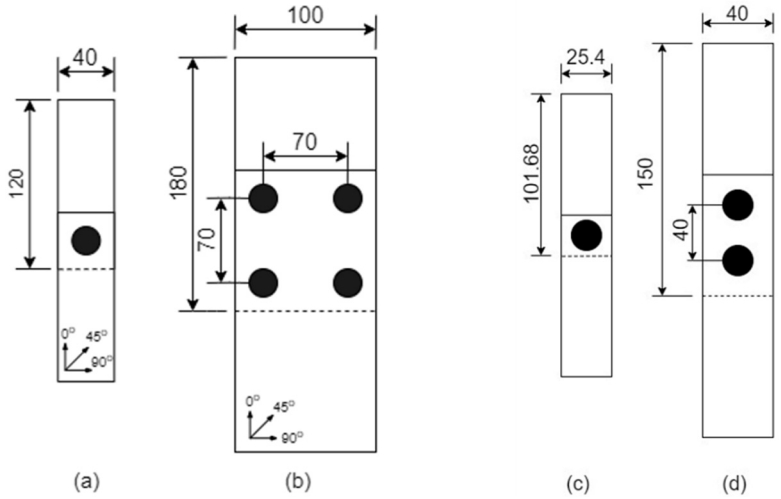

Figure 3. Schematic representation of all types of ultrasonic-welded coupons produced during this study. (**a**) Cross-ply UD CF/LMPAEK to cross-ply UD CF/LMPAEK single spot; (**b**) cross-ply UD CF/LMPAEK to cross-ply UD CF/LMPAEK multi-spot, welded in an anti-clockwise sequence starting from top left; (**c**) SF CF/LMPAEK to quasi-isotropic UD CF/LMPAEK single spot; and (**d**) SF CF/LMPAEK to quasi-isotropic UD CF/LMPAEK multi-spot joint, welded in a top-to-bottom welding sequence.

2.1.2. Ultrasonic Welding

Reference Table-Top Static Welder

To create reference welds, an off-the-shelf table-top welding machine called Dynamic 3000 from Rinco Ultrasonics (Romanshorn, Switzerland) was utilized (shown in Figure 4a), operating at a frequency of 20 kHz. The welding machine consists of the standard components, including an ultrasonic welding stack composed of a converter, booster, and sonotrode, operated by a pneumatic press. This static welding machine is designed with an

encapsulated and clamped ultrasonic stack, housed in a closed box carriage on rails. To produce circular welded spots, a cylindrical titanium sonotrode with a diameter of 20 mm was employed.

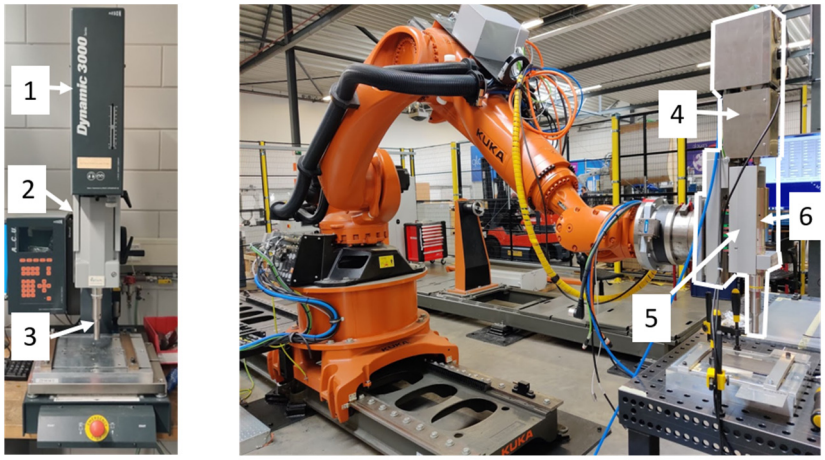

Figure 4. (**a**) Static table-top welding machine. (1) Pneumatic press; (2) closed box carriage on rails; (3) ultrasonic stack with sonotrode visible. (**b**) EEF setup outlined in white on an industrial KUKA robot. (4) Pneumatic press; (5) open box carriage on rails; (6) ultrasonic stack. Reproduced with permission from [13].

Each spot was welded using a welding force of either 800 N (for UD-to-UD welds) or 850 N (for SF-to-UD welds) and a peak-to-peak vibration amplitude of 65.8 µm, as determined in a preliminary study [13]. The difference in welding force between the two configurations can be attributed to the differences in compliance of the energy directors used for the UD-to-UD and the SF-to-UD welds. The optimal vibration time for each spot was found to be dependent on the adherends' size, material configuration, and the weld's location within the overlap. Determining the optimum vibration time involved a combination of trial-and-error analysis of time-resolved power and vertical displacement feedback obtained from the welder [4], along with the examination of the fracture surfaces and micrographs of the resulting welds. After the vibration phase, the weld was allowed to cool down under 800 N of consolidation force for a certain time (consolidation phase). Owing to differences in heat transfer, different consolidation times of 6 s and 10 s were used for the UD-to-UD and the SF-to-UD welds, respectively. This variation in consolidation time ensured that the weld cooled down sufficiently before pressure was removed to avoid deconsolidation. Table 2 lists the welding parameters for all the configurations researched in this study. To hold the specimens securely in position during welding, a bar-clamp jig was employed. A time-controlled welding mode was employed for procuring the welds. The static multi-spot welds produced with the static table-top machine required manually moving the adherends on the jig relative to the fixed position of the sonotrode for sequential production of the welds.

Table 2. Welding parameters per weld configuration.

Material Configuration	Weld Configuration	Welding/Consolidation Force (N)	Vibrational Amplitude (µm)
UD CF/LMPAEK to UD CF/LMPAEK	Single-spot	800	65.8
	Multi-spot	800	65.8
SF CF/LMPAEK to UD CF/LMPAEK	Single spot	850	65.8
	Multi-spot	850	65.8

Industrial Robot-Based Welder

The robotic welding setup used in this part of the work consisted of a generic end-effector (EEF) attached to a KUKA KR210 R2700 Extra industrial robot arm (shown in Figure 4b), which was acquired from KUKA AG (Augsburg, Germany). The EEF incorporates an ultrasonic stack fixed onto an open box carriage, which was mounted on linear guide rails and operated by a pneumatic press with a maximum force of 2 kN. A 20 kHz Rinco Ultrasonics generator with a maximum power output of 3 kW was employed to generate ultrasonic signals.

The welding force, consolidation force and amplitude of vibration were the same as in the static table-top welding process. The same bar-clamp jig was used in the robotic welding process; however, for the sequentially welded joints, the robot arm and hence the attached EEF moved relative to the fixed weld jig in order to sequentially position the sonotrode above the intended weld spot(s). The general position of the robot during the welding experiments conducted in this study can be seen in Figure 4b, with the EEF positioned perpendicularly above the surface of the welding jig and welding table. The robot was programmed to ensure that the sonotrode remained perpendicular to the adherends when the arm moved to reach each welding position.

2.1.3. Data Capture and Analysis Techniques

The vertical displacement of the ultrasonic welding stack (once situated at the welding position) was measured via an internal displacement sensor in both the table-top and robotic welding machines and recorded at a sampling rate of 1 KHz. Additionally, the ultrasonic generator recorded the power and energy dissipated during the welding process at a sampling rate of 100 Hz. The vertical displacement of the welding stack and the power and energy consumed during the welding process provide information about melting and squeeze flow during the ultrasonic welding process [5].

To assess the mechanical performance of the welded joints, tensile tests were performed in single-lap shear configuration in a Zwick/Roell 250 kN universal testing machine provided with hydraulic grips, operated at a 1.3 mm/min crosshead speed (displacement control). Five samples were tested per single-spot and multi-spot welding configuration for each of the processes (table-top and robot-based welders). While no specific standard was followed due to the non-conventional coupon dimensions, the test method was aligned with ASTM D1002 as closely as possible.

The single-lap shear strength (SLSS) was calculated by dividing the maximum load registered in the test by the total welded area. The total welded area for each sample was measured by analyzing the fracture surface area using a Keyence VR-3000 One-shot 3D Measuring Microscope. To further analyze the quality of the welded joint, two analysis techniques were employed: ultrasonic through-transmission C-scan inspection and cross-sectional microscopy. For the C-scan analysis, an Olympus (Tokyo, Japan)—OmniScan SX was utilized to scan the samples, which were submerged in a water tank. For the cross-section analysis, the overlap was cut along the longitudinal direction of the adherends, precisely at the center of the adherends' width. Subsequently, the samples were embedded in epoxy resin and polished using a Struers (Ballerup, Denmar)—Tegramin-20 polisher. To observe and analyze the cross-sections, a Keyence (Osaka, Japan) VH-Z100 digital microscope was employed.

2.1.4. Test Matrix

Table 3 shows an overview of the different coupon-level welded joints with varying material configurations that were produced with the static table-top and robot-based welding machines.

Table 3. Summary of tests performed at coupon level.

Type of Joint	No. of Weld Spots	Layup of UD Coupon	ED Type	Welding Machine	No. of Samples	Purpose
Single spot (UD to UD)	1	Cross-ply	Discontinuous ED (0.32 mm thick)	Table-top/robot-based	10	Comparison of robot and table-top welding process
Multi-spot (UD to UD)	4	Cross-ply	Discontinuous ED	Table-top/robot-based	5	
Single spot (SF to UD)	1	Quasi-isotropic	Molded riblets on SF coupon	Table-top/robot-based	10	Comparison of robot and table-top welding process for different material configuration
Multi-spot (SF to UD)	2	Quasi-isotropic	Molded riblets on SF coupon	Table-top/robot-based	4	

2.2. Results

Figure 5 provides a comparison of the total welded area, ultimate failure load, and lap shear strength of the single-spot and multi-spot joint configurations using the table-top and robot-based welding processes to create UD-to-UD CF/LMPAEK welds. In most cases, the welded spots had a somewhat elliptical shape, and in all cases, failure was observed to occur in the first ply adjacent to the weld interface (Figure 6). The spot welds produced with the robotic setup were found to horizontally shift by approximately 1 mm with respect to the programmed position due to suspected deflection of the robotic welding system [13]. The observed shift in the position of the welded spot was attributed to two factors: deflection of the robot and bending of the welding end-effector under the applied welding force. To mitigate the former, the robot base, which was mounted on a movable linear track, was repositioned closer to the welding jig. However, this strategy did not have an influence on the horizontal shift of the welded spot. The latter factor, bending of the end-effector, was a result of the design of the generic welding end-effector which was not further modified for the coupon-level study. No horizontal shift of the weld spot was observed in the welds produced with the table-top welder.

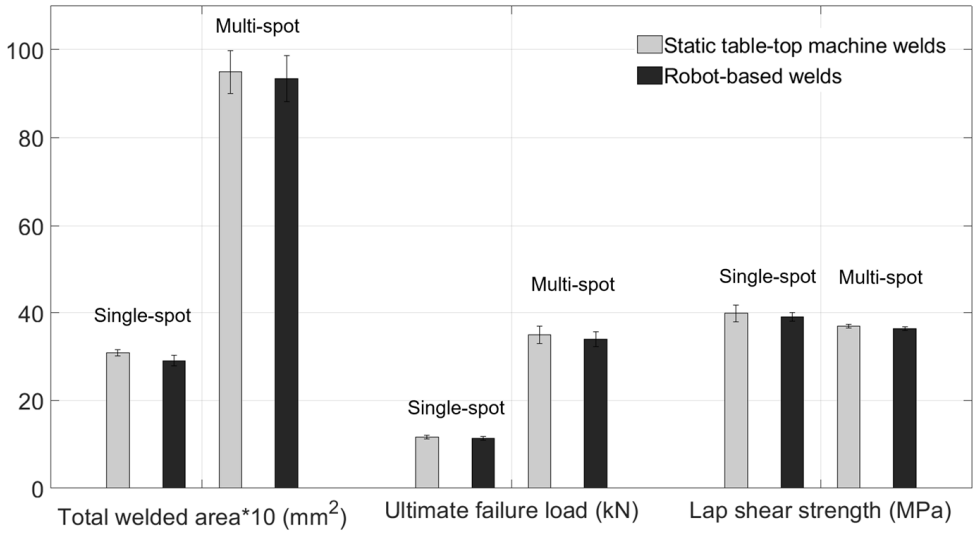

Figure 5. Comparison of total welding area, ultimate failure load and lap shear strength for single-spot and multi-spot UD-to-UD CF/LMAPEK welding configurations with the table-top and the robot-based welds.

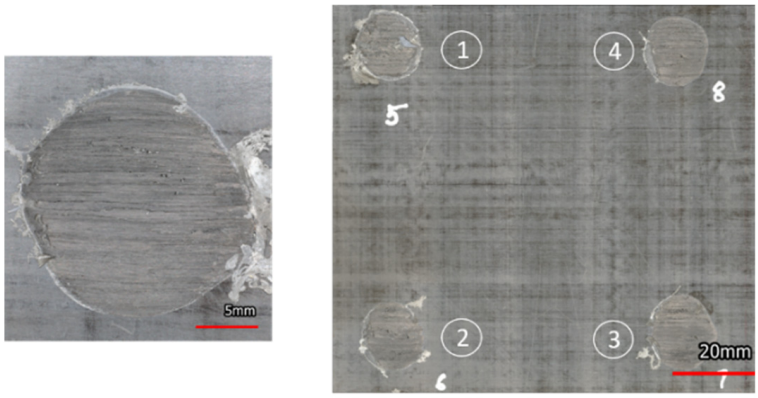

Figure 6. Representative UD-to-UD weld fracture surfaces obtained after single-lap shear testing in (**a**) single-spot configuration and (**b**) multi-spot configuration with weld sequences denoted as 1, 2, 3, and 4, respectively. Welds were produced with the robot-based welder. Reproduced with permission from [13].

In the case of the SF-to-UD CF/LMPAEK welds, all the welded coupons experienced adherend failure at the edge of the overlap within the short-fiber CF/LMPAEK adherend (Figure 7) upon mechanical testing, rather than at the weld interface, which indicates a high joint strength. The actual welded area was not measured. The mechanical testing results can be seen in Table 4. Cross-sectional microscopy revealed uniform and a porosity-free weld interface (Figure 8) between the SF CF/LMPAEK and the UD CF/LMPAEK coupons. Figure 9 shows representative C-scan images of this type of welded joint.

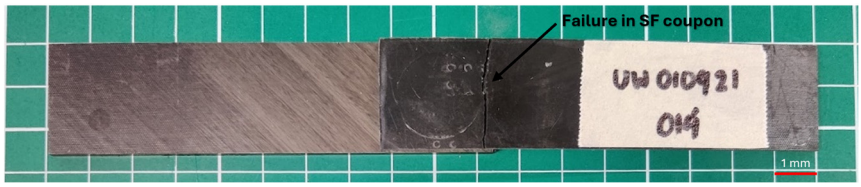

Figure 7. Representative SF-to-UD CF/LMPAEK single-spot welded coupon after mechanical testing showing failure in the short-fiber-reinforced coupon. Weld produced with the robot-based process.

Table 4. Mechanical testing results of SF-to-UD CF/LMPAEK welds.

Weld Configuration	Material Configuration	Ultimate Failure Load (N)	Standard Deviation (N)
Single Spot	SF CF/LMPAEK to UD CF/LMPAEK	5270	200
Multi-spot	SF CF/LMPAEK to UD CF/LMPAEK	8914	420

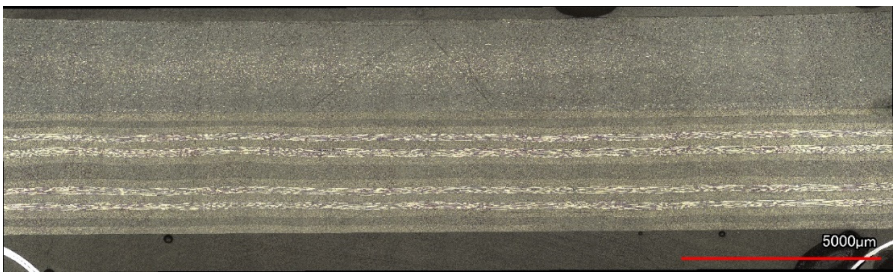

Figure 8. Representative cross-sectional micrograph of a welded joint with SF CF/LMPAEK coupon as top adherend and UD CF/LMPAEK coupon as bottom adherend. Weld produced with the robot-based process.

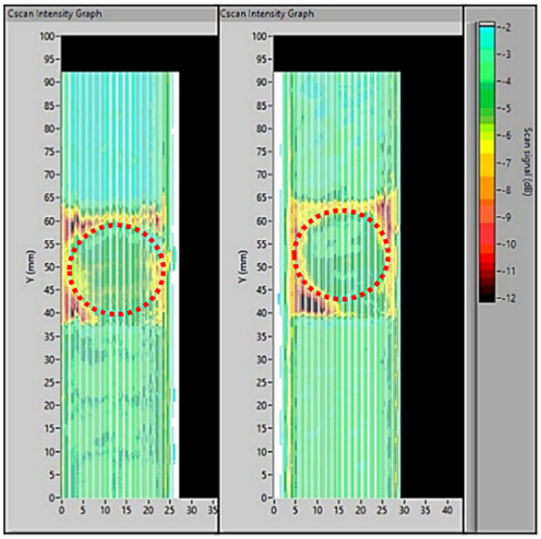

Figure 9. Representative C-scan images of SF-to-UD CF/LMPAEK single-spot welds (sonotrode footprint indicated with red circles). Welds produced with the robot-based process.

The welding (vibration) times used to obtain these results in each of the welding configurations are shown in Table 5.

Table 5. Vibration times for all welding configurations.

Weld Configuration	Material Configuration	Vibration Time (Table-Top) (ms)	Vibration Time (Robot-Based) (ms)
Single Spot	UD CF/LMPAEK to UD CF/LMPAEK	800	850
Multi-spot		Spot 1: 1250 Spot 2: 1300 Spot 3: 1350 Spot 4: 1400	Spot 1: 1400 Spot 2: 1450 Spot 3: 1500 Spot 4: 1550
Single spot	SF CF/LMPAEK to UD CF/LMPAEK	800	800
Multi-spot		Spot 1: 800 Spot 2: 850	Spot 1: 800 Spot 2: 850

2.3. Discussion

The results shown above indicate that the robot-based ultrasonic spot welding process can produce high-quality single- and multi-spot welds for both material combinations researched in this study. It was found that the ultimate failure load, welded area, and lap-shear strength in the case of welds produced in the UD-to-UD CF/LMAPEK coupons were similar, with no statistically significant differences between the static and robot-based welding processes (Figure 5). These results indicate that in future applications of ultrasonic spot welding on large-scale thermoplastic composite structures, it might be possible to define an initial set of welding process parameters using laboratory-scale equipment, which might only require small modifications for full-scale application. It should, however, be noted that the preliminary definition of the welding parameters should be carried out by reproducing the final boundary conditions as much as possible. Indeed, as shown in Table 5, actions such as increasing the width of the overlap (e.g., differences between the single-spot weld and spot 1 in the multi-spot configuration in UD-to-UD welds) or gradually increasing stiffness of the overlap (e.g., differences among consecutive spots in multi-spot welds) have a significant effect on the required vibration time and consequently the energy required to produce a welded joint.

As shown in Tables 2 and 5, the welding parameters may differ slightly between the table-top and robot-based welding processes. The observed slight increase in the required vibration time for the robot-based process in the case of UD-to-UD welds might be attributed to the extra time required for the sonotrode to horizontally shift to its final position. This horizontal shift of about 1 mm, as mentioned earlier, was observed after the onset of sonotrode vibrations. This is suspected to result in some dissipation of weld energy, necessitating a longer vibration time. The above-mentioned horizontal shift is consistent with the lower stiffness of the KUKA robot compared to the table-top welding machine and could potentially be minimized by using stiffer equipment. Note that in the case of the SF-to-UD welds, the vibration times required for both table-top and robot-based welding were, however, the same. The lower hardness of the SF CF/LMPAEK material resulted in a slight penetration of the sonotrode on the top surface of the top adherend (evidenced by the slight imprint observed in Figure 7), which most likely locked the sonotrode into its original position, preventing any horizontal shifts after the onset of the vibration.

High weld quality was evidenced in the case of the UD-to-UD CF/LMPAEK welds by the occurrence of first-ply failure (Figure 6) and the resulting welded areas amounting to 81% of the area of the sonotrode (Figure 5). In the case of the SF-to-UD CF/LMPAEK welds, high weld quality was indicated by a low signal attenuation area in the C-scan images, similar to the footprint of the sonotrode (Figure 9) and by cross-sectional images indicating no porosity within the welded spot (Figure 8). It should be noted that the ultimate load of these welded joints (single spot) was approximately half of that of UD-to-UD single-spot welds (Figure 5). However, this cannot be taken as a measure of quality given the fact it was not the SF-to-UD welds that failed during the tensile tests but the short-fiber-reinforced adherends themselves (Figure 7).

3. Part II: Full-Scale Demonstrator

The first section of this paper highlights similarities in welding parameters and performance between the table-top and robot-based welding processes. The small variation in welding parameters between the two processes also highlights the challenges posed by the robot-based welding system, including limited stiffness and positioning inaccuracies. These findings were carefully considered in designing and implementing the ultrasonic welding setup for the full-scale demonstrator. For motion automation, a gantry robot was designed and implemented with a payload capacity of 450 kg (higher than the KUKA KR210 robot at 210 kg) and a working area of 9.1 m $\times$ 7.1 m. This enabled the gantry robot to grip the welding end-effectors and accurately position them at all weld locations in the demonstrator. Based on the deflections observed within the frame of the generic welding end-effector used in Part I of this work, the end-effectors were designed and constructed with a stiffer frame and with specific clamping tools for the automated welding operations. This stiffer frame allowed for a maximum deflection of 0.02 mm within the end-effector at a maximum welding force of 1500 N. Furthermore, the welding parameters for the full-scale demonstrator were derived from those established for welding SF CF/LMPAEK-to-UD CF/LMPAEK coupons using the robot-based welding process described in Part I.

3.1. Description of Parts and Welding System

3.1.1. Materials, Part Manufacturing, and Geometry

Sequential ultrasonic welding was used in the lower shell of the MFFD demonstrator to assemble the 12 circumferential frames to the stiffened skin through a total of 212 structural clips. The fuselage skin is 8.0 m in length and 4.0 m in diameter and has varying thicknesses ranging from 2.2 mm to 9 mm. It was manufactured from CF/LMPAEK UD tape material from Toray Advanced Composites using automated fiber placement at the Netherlands

Aerospace Center–NLR (Marknesse, The Netherlands), followed by autoclave consolidation at the German Aerospace Center—DLR (Stade, Germany) [12]. After consolidation, the skin was placed on a welding jig, which acted as a female mold for the following sub-assembly steps. The skin was stiffened with omega stringers produced with UD CF/LMPAEK, which were 1.65 mm thick and joined to the skin using conduction welding [16]. The circumferential frames had a C-shaped cross-section with a web approximately 2.2 mm thick. They were also produced out of CF/LMPAEK UD tape material (TC1225) using the butt-joint technology developed by GKN-Fokker (Hogeveen, The Netherlands) [12]. The clips were designed to make contact with the skin, stringer feet, and the web of the frame, as shown in Figure 10. They were produced using recycled, short-fiber CF/LMPAEK with a 40% fiber volume fraction through injection molding by the AITIIP Technology Centre, Spain [15]. The welding surfaces of the clips had a thickness of 3.8 mm and energy directors consisting of triangular ridges, such as the ones shown in Figure 2, molded onto them. The choice to incorporate triangular energy directors onto the welding interface was to allow for one-shot injection molding of the short-fiber CF/LMPAEK. For each welding spot, the energy director covered a circular area 23 mm in diameter. It is important to note that the clips were manufactured such that the bottom flanges were not flat and conformed to the curvature of the skin.

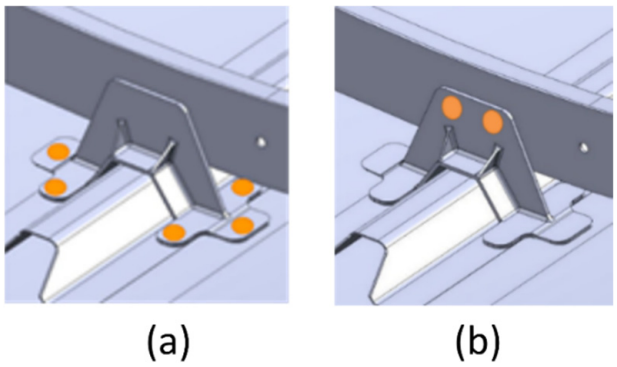

Figure 10. Joint configuration for (**a**) spot welding of the clip to skin/stringer and for (**b**) spot welding the clips to the frame coupling.

3.1.2. Welding

Assembly of the circumferential frames to the stiffened skin was divided into two welding steps: (a) clip-to-skin (CTS) welding step consisting of ultrasonic welding of the clip feet to the stiffened skin panel with two welding spots on the skin and four on the flanges of the omega stringer, as depicted in Figure 10a and (b) frame-to-clip (FTC) welding step consisting of ultrasonic welding of the vertical flange of the clips to the web of the frame with two adjacent welding spots, as depicted in Figure 10b. To join all parts together, a total of eight welded spots were produced on each clip, resulting in a total of 1696 ultrasonic spot welded joints on the demonstrator. The CTS welding operation involved six welded spots per clip. The outer feet of the clip that make contact with the skin directly were welded first. Subsequently, the remaining four spots on the clip–stringer interface were welded. The welding sequence can be seen in Figure 11a, depicted by the numbers 1–6. This sequence was chosen since it helped mitigate the risk of misalignment of the clip with respect to the frames due to potential gaps between the stringers and the clip feet. The first two spot welds ensured perfect alignment of the clip with respect to the skin surface and mitigated the risk of clip rotation during the spot welding sequence. This also ensured that the vertical flange of the clip that would mate with the frame was perfectly aligned. Following this, the spot welds at locations 3, 4, 5, and 6 were produced in the corresponding sequence. This ensured that the clip would not undergo torsion due

to the presence of varying misalignment or gaps between the clip and the stringer at the remain spots, and which may result in peel stresses acting on the welded joints due to residual stresses after welding. An alternate welding sequence may influence the weld quality by altering the residual stress release during the process; however, this was not experimentally validated. The sequence of welding the two spots on the clip-to-frame interface (spots 1 and 2 in (Figure 11b)) does not matter from the welding process point of view. Hence, a sequence was chosen based on the ease of robot motion.

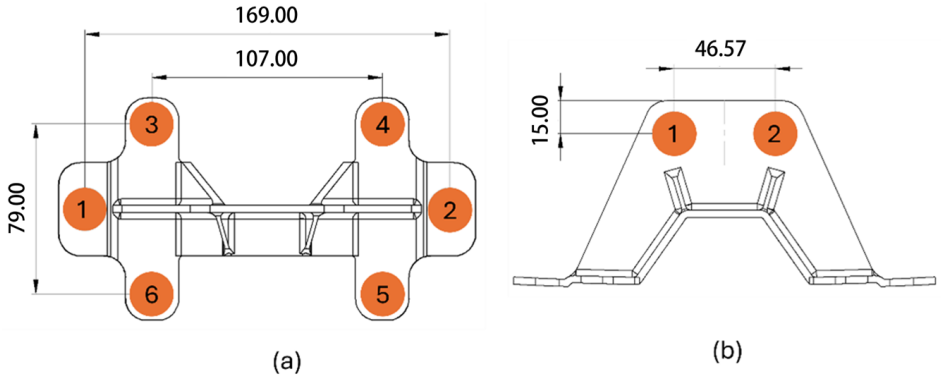

Figure 11. Sequential spot welding sequence for (**a**) the clip, skin, and stringer joint, and (**b**) clip and frame joint (dimensions are in mm).

To automate the spot welding process, a specific welding end-effector (EEF) was developed and mounted on the wrist of an overhead gantry robot. The gantry robot was developed as a generic motion platform for research projects on manufacturing large components. SAM XL defined the specifications of the gantry robot, while the system was designed and built by Vansichen (Hasselt, Belgium). The gantry robot offers 6 degrees of freedom (XYZ translation and rotation), while the wrist allows for two additional rotations. This allows the EEF to reach all locations in the demonstrator and to position the sonotrode perpendicular to the clip at the welding locations for both the CTS and FTC welds.

The EEF was designed to be compatible with two different welding tools, which were specifically designed and built for CTS and FTC welding (Figure 12). Similar to the setup shown in Figure 4b, the CTS welding tool (Figure 12) relies on the welding stack being actuated vertically, normal to the parts to be welded and to the welding jig on which the stiffened skin was positioned. It includes a pneumatically actuated picture-frame clamp that is used to restrict any in-plane movement of the clip flange at the weld spots 1 and 2, during the welding operation. The frame-to-clip (FTC) welding tool (Figure 13) includes an integrated anvil to provide back pressure on the frame during the welding process, since the vertical flange of the clip needs to be welded to the vertical flange of the frame, which is not supported by any external tooling. However, additional clamps to prevent sliding between the frame and clip were not required since the frame was clamped in its position in the fuselage barrel, and the clips were welded to the skin and stringer in the previous step. It should be noted that due to the large number of welds and the tight tolerances required between the parts themselves, as well as between the sonotrode and the part, it was critical to carefully integrate the EEF with the gantry robot and calibrate the welding tool with respect to the stiffened skin and frames.

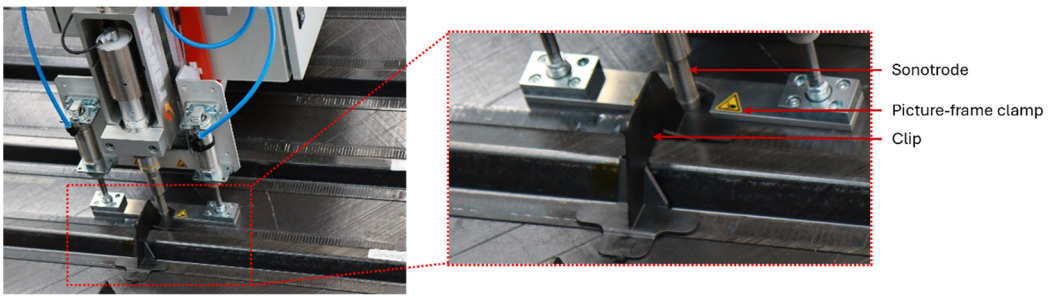

Figure 12. CTS welding tool with the picture-frame clamp.

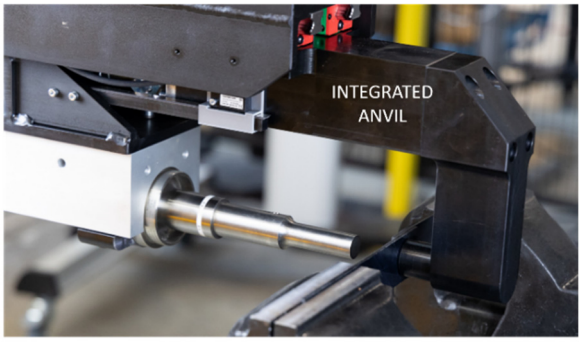

Figure 13. FTC welding tool with the integrated anvil.

The welding force, amplitude of vibration, and consolidation force defined in Part I of this research for the SF CF/LMPAEK-to-UD CF/LMPAEK welds were maintained for welding of the clips to the skin and the frames to the clips. The vibration time and consolidation time were, however, varied. For the vibration time, adjustments were made for each weld location on a clip to account for evolving boundary conditions, reduced part compliance, and the presence of additional polymer layers for gap management, thereby resulting in eight parameter sets per clip. These parameter sets were initially established during laboratory experiments and later updated on a case-to-case basis for the clips installed in the demonstrator. During the assembly process, the consolidation time varied between 6 and 10 s to ensure that sufficient heat dissipation took place before the consolidation force was removed, avoiding de-consolidation of the weld or the bulk material. During the ultrasonic welding process, the welding equipment recorded the power consumed to maintain the specified vibration during welding, the force applied by the robotic arm on the welding stack, and the displacement of the sonotrode relative to the robotic arm, as measured by the displacement sensor of the welding stack. These are referred to as the welding data. During the sequential spot welding process in the demonstrator, the welding data was recorded with the intention of obtaining extra information about the welding process.

3.2. Results and Discussion

Figure 14 shows the lower shell of the MFFD demonstrator after welding the 212 clips to the skin and stringer flanges and Figure 15 shows it after welding the 12 frames to the clips. Table 6 shows the vibration time ranges used for the eight clip spot welds.

Compared to the robot-based welding trials conducted in Part I of this study, no horizontal shift in the weld spot was observed for the welded joints produced in the demonstrator. This outcome indicates that the combined stiffness of the gantry robot system and end-effector design was sufficient to achieve the required positional accuracy.

Figure 14. The lower shell of the MFFD demonstrator after welding the clips to the skin and stringer.

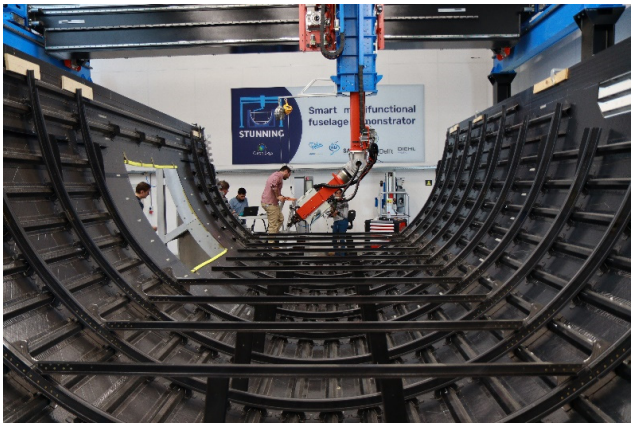

Figure 15. The lower shell of the MFFD demonstrator after welding the frames to the clips.

Table 6. Vibration times for clip welds.

Weld Position	Vibration Time Range (ms)
CTS Spot 1	1200–1400
CTS Spot 2	1200–1400
CTS Spot 3	1350–1500
CTS Spot 4	1350–1500
CTS Spot 5	1350–1500
CTS Spot 6	1350–1500
CTF Spot 1	1350
CTF Spot 2	1400

During the assembling process, various gaps and misalignments were observed between the parts to be welded, in particular at the CTS welds. The gaps and misalignment between the welding interfaces were built-up tolerances resulting from local deformation of the parts during the preceding manufacturing steps, including skin manufacturing and conduction welding of the stringers. The vertical gaps between the clip feet and stringer or skin ranged from 1 mm to 9 mm. To be able to compensate for this vertical gap between the parts, shims had to be used, and the vibration time had to be varied. These shims consisted of multiple layers of the discontinuous LMPAEK film stacked on top of each other, like those used in Part I of this research, and placed in between UD mating parts prior to the welding process. Each layer of the discontinuous LMPAEK film was 0.3 mm thick. These shims acted as additional ED which melted during the welding process resulting, in some cases, in significant resin flash at the edges of the feet of the clips due to squeeze flow and relatively resin-rich weld lines, as depicted in Figure 16. This figure shows a cross-section micrograph

of a weld between a clip foot and a flat panel obtained in a laboratory trial in which two shim layers were placed between the two welding surfaces prior to the welding process. It should be noted that when shims were used, due to the higher compliance of the shims as compared to the energy director ridges, partially intact ridges can be seen at the weld interface. For comparison purposes, Figure 17 shows a cross-section micrograph of a weld between a clip and a flat panel from the same trial in which no extra shims were used. It should be noted that the positioning of the LMPAEK shims to close the gaps was performed manually. Together with the measurement of all actual clip positions, which significantly deviated from the digital model of the demonstrator, this resulted in a semi-automated rather than a fully automated assembling process. In general, for spot welds where large gaps were observed and multiple shim layers had to be placed, a longer vibration time was required to generate sufficient heating at the interface to melt the material.

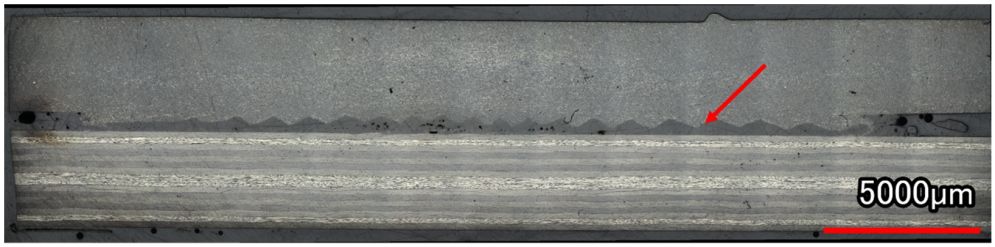

Figure 16. Cross-sectional micrograph of welded joint between clip (upper part) and flat skin panel (lower part) with 2 shim layers. Red arrow indicates the weld line, which exhibits partially intact energy director ridges and a resin-rich area between the clip and skin panel.

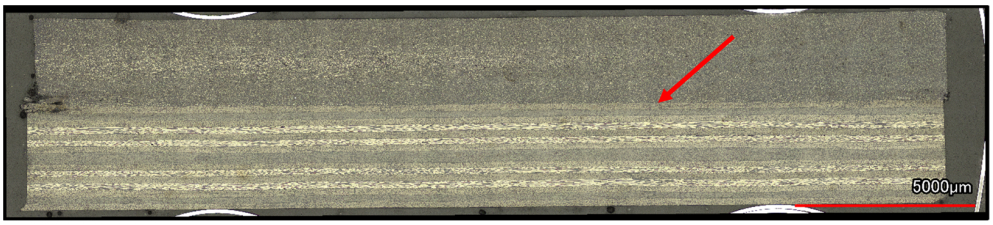

Figure 17. Representative cross-sectional micrograph of welded joint between clip (upper part) and flat skin panel (lower part) of the micrograph, with no shim layers. Red arrow indicates the weld line, which contains no excess resin.

Due to the compliance of the short-fiber-reinforced material of the clips in combination with the shims used, most gaps could be visually closed under pressure application from the sonotrode, and the parts could be welded. However, this is suspected to have caused an uneven cyclic strain distribution, which could have resulted in uneven heating [17] and eventually a deviation in weld quality from what was expected. The vibration time required to achieve sufficient heating at the interface to form a welded joint varied based on the number of shim layers used. The vibration time was determined experimentally. It is also suspected that the joints entrapped high internal stresses due to being forced into position. Finally, the sonotrode caused indentations on the clip material at the welding spots, which featured the largest gaps and consequently required more shim layers to fill the gaps. On the contrary, no gaps or misalignments were observed between the frames and the clips; hence, no shims were necessary for the FTC welds, and the clips showed only minimal imprints of the sonotrode at the welding locations.

3.3. Analysis of Welding Data

The displacement of the sonotrode perpendicular to the welding surfaces during the welding process provides an indication of the magnitude of the gaps existing in between the welding surfaces. It should be noted that this displacement, however, was measured

by the ultrasonic welder from the moment at which the full welding force was applied. Figures 18–20 show maps of the displacement of the sonotrode during the welding process for CTS welds (spot 1: weld between clip foot and skin, and spot 5: weld between clip foot and stringer flange, see Figure 10) and for FTC welds, respectively. It should be noted that because the consolidation time of the welds ranged between 6 and 10 s, a decision was made to compare the displacement values at 6 s from the start of the welding process. However, no significant variation in displacement was observed beyond 6 s in any of the welds. It should also be noted that the locations in the maps that show nil displacement correspond to locations with no clips or with clips for which the weld data was either not available or incomplete and were omitted from the analysis. As seen in these Figures, the displacement values for the FTC welds (Figure 20), and therefore the gaps, are much smaller and more uniform than those for the CTS welds (Figures 18 and 19). Within this last category, the welds between clip foot and skin (Figure 18) show smaller and more uniform displacement values than the welds between clip foot and stringer flange (Figure 19). This is consistent with the significant indentation caused in the stringer flanges because of the conduction welding process.

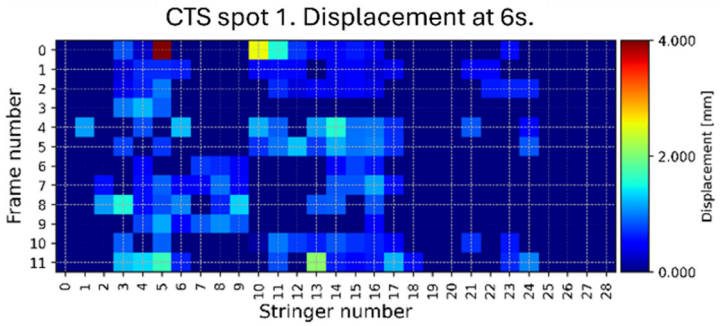

Figure 18. Recorded displacement of the sonotrode during the CTS welding process at spot number 1 (clip foot to skin) according to the welding sequence depicted in Figure 11.

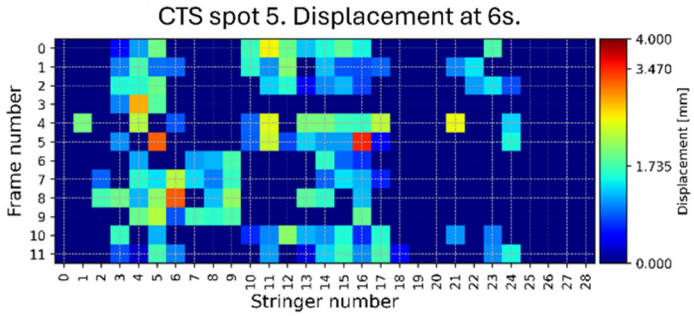

Figure 19. Recorded displacement of sonotrode during the CTS welding process at spot number 5 (clip foot to stringer flange weld) according to the welding sequence depicted in Figure 11.

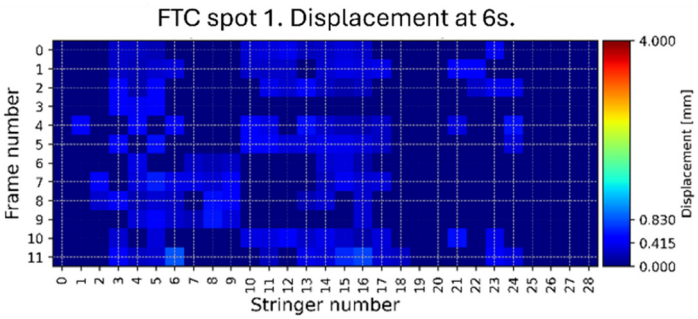

Figure 20. Recorded displacement of the sonotrode during the FTC welding process.

The energy consumed by the ultrasonic generator to create the ultrasonic weld spots gives an indication of the weld quality. As shown in Figure 21, the energy consumed by the CTS welds was consistently lower than that consumed by the FTC welds. The lower energy of CTS welds is consistent with the results obtained in previous studies on welding of misaligned adherends [17], which also show a decrease in the weld quality as the misalignment increases. In general, the CTS welds featured larger gaps and therefore required more shim layers to close the gap. Due to the higher amount of resin-rich material at the interface, they are suspected to have higher compliance to ultrasonic vibration and therefore require lesser energy for sufficient heat generation at the interface.

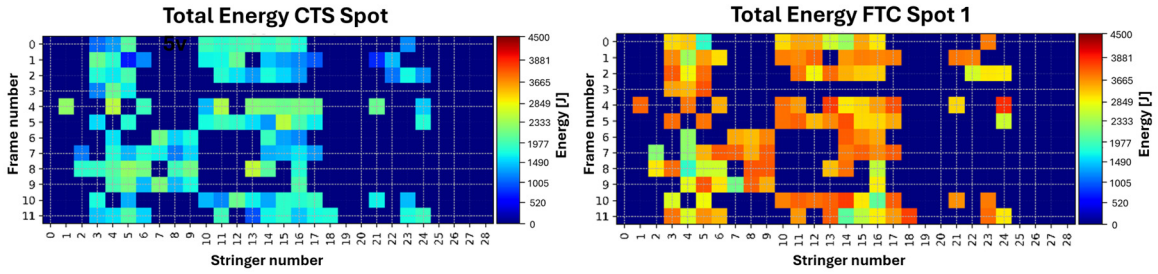

Figure 21. Energy consumed for CTS compared to the energy consumed for FTC welding.

4. Conclusions

This paper highlights the process development steps that have been taken at SAM XL and Delft University of Technology to realize an automated sequential ultrasonic spot welding process, which was demonstrated on the lower shell of the Multi-Functional Fuselage Demonstrator (MFFD). The main conclusions of the first step, an experimental comparison between table-top and robot-based approaches for the creation of single- and multi-spot welded joints at the coupon level and in different material combinations, were that both processes can provide welds of similar quality using similar welding parameters. Furthermore, the study highlighted the main challenges posed by the robot-based welding system, namely limited stiffness and position inaccuracies. The study also underscored the challenges of applying this process to large structures for sequential spot welding, particularly in maintaining consistent boundary conditions across different weld locations. Variations in overlap stiffness at these locations necessitated adjustments in vibration time to ensure sufficient heat generation and thus uniform weld quality. The main conclusions of the second step, i.e., application of robotic ultrasonic welding to the assembling of skin and frames in the MFFD, were that, with the development of two dedicated end-effectors and the use of an overhead gantry robot with a larger payload, the process could be applied for the joining of structural components in a full-scale demonstrator. Additionally, our activities showed that the weldabilty of structures through the ultrasonic spot welding process is highly dependent on gaps, tolerances, and surface quality of the parts. Industrialization of the ultrasonic welding process for the joining of structures should take into account the reachability of weld surfaces, deformation of parts, and process tolerances. Although gaps of up to 9 mm between the clips and stringer could be closed due to the use of shims and the compliance of the short-fiber-reinforced clips, the resulting weld likely contains a resin-rich interface and significant entrapped residual stresses, both of which can adversely influence joint strength. Future work should focus on defining the maximum process tolerance to gaps, misalignments, and surface roughness, which is expected to be unique for each material type, fiber architecture, part compliance, joint type, and geometry of the energy director. Furthermore, due to the high process forces involved, the stiffness of the chosen industrial robot system, as well as the stiffness of the back support structure, play an important role in the success of the upscaling of the welding process. As witnessed,

while applying a maximum process force of 850 N, the position of the welding end-effector shifted horizontally by 1 mm while using the KUKA robot with a generic end-effector. Such displacement would be unacceptable in a production environment. Overall, the results achieved in this work demonstrate the strong potential of ultrasonic spot welding to be used as a very fast structural joining method for airframe parts and show the feasibility of automating the process using robotic systems to increase aircraft production rates in the future.

Author Contributions: A.C.: Writing—original draft, Visualization, Methodology, Investigation, Formal analysis, Conceptualization. I.B.-A.: Writing—review and editing, Visualization. I.F.V.: Writing—original draft, Supervision, Funding acquisition, Data curation, Conceptualization. All authors have read and agreed to the published version of the manuscript.

Funding: This research was funded by the European Union's Clean Sky 2 Joint Undertaking (JU) under grant agreement No 945583. The JU receives support from the European Union's Horizon 2020 research and innovation program and from the non-EU Clean Sky 2 JU members. The APC was funded by the Delft University of Technology.

Data Availability Statement: The original contributions presented in this study are included in the article. Further inquiries can be directed to the corresponding author.

Acknowledgments: The results, opinions, conclusions, etc. presented in this work are those of the authors only and do not necessarily represent the position of the JU; the JU is not responsible for any use made of the information contained herein.

Conflicts of Interest: The authors declare that they have no known competing financial interests or personal relationships that could have appeared to influence the work reported in this paper.

References

1. Multi-Functional Fuselage Demonstrator. Available online: https://www.clean-aviation.eu/clean-sky-2/key-demonstrators/multi-functional-fuselage-demonstrator (accessed on 15 February 2025).
2. Fantastic Thermoplastics: Novel Techniques and Materials are Accelerating a Rethink of Aerostructure Production. Available online: https://www.airbus.com/en/newsroom/stories/2025-01-fantastic-thermoplastics (accessed on 15 February 2025).
3. Manufacturing the MFFD Thermoplastic Composite Fuselage. Available online: https://www.compositesworld.com/articles/manufacturing-the-mffd-thermoplastic-composite-fuselage (accessed on 14 July 2023).
4. Ageorges, C.; Ye, L.; Hou, M. Advances in fusion bonding techniques for joining thermoplastic matrix composites: A review. *Compos. Part A Appl. Sci. Manuf.* **2001**, *32*, 839–857. [CrossRef]
5. Villegas, I.F. Strength development versus process data in ultrasonic welding of thermoplastic composites with flat energy directors and its application to the definition of optimum processing parameters. *Compos. Part A Appl. Sci. Manuf.* **2014**, *65*, 27–37. [CrossRef]
6. Grewell, D.; Benatar, A.; Park, J.B. *Plastics and Composites Welding Handbook*; Carl Hanser Verlag: Munich, Germany, 2003; Volume 10, p. 10.
7. Benatar, A.; Eswaran, R.V.; Nayar, S.K. Ultrasonic welding of thermoplastics in the near-field. *Polym. Eng. Sci.* **1989**, *29*, 1689–1698. [CrossRef]
8. Liu, S.-J.; Chang, I.-T.; Hung, S.-W. Factors affecting the joint strength of ultrasonically welded polypropylene composites. *Polym. Compos.* **2001**, *22*, 132–141. [CrossRef]
9. Benatar, A.; Gutowski, T.G. Ultrasonic welding of PEEK graphite APC-2 composites. *Polym. Eng. Sci.* **1989**, *29*, 1705–1721. [CrossRef]
10. Zhang, Z.; Wang, X.; Luo, Y.; Zhang, Z.; Wang, L. Study on Heating Process of Ultrasonic Welding for Thermoplastics. *J. Thermoplast. Compos. Mater.* **2009**, *23*, 647–664. [CrossRef]
11. Zhao, T.; Rans, C.D.; Villegas, I.F.; Benedictus, R. On sequential ultrasonic spot welding as an alternative to mechanical fastening in thermoplastic composite assemblies: A study on single-column multi-row single-lap shear joints. *Compos. Part A Appl. Sci. Manuf.* **2019**, *120*, 1–11. [CrossRef]
12. Veldman, S.L.; Kortbeek, P.; Wölcken, P.C.; Herrmann, R.; Kos, J.; Villegas, I.F. Development of a multifunctional fuselage demonstrator. In Proceedings of the Aerospace Europe Conference, Bordeaux, France, 25–28 February 2020.

13. Choudhary, A.; Villegas, I.F. Robotic sequential ultrasonic welding of thermoplastic composites: Process development and testing. In Proceedings of the American Society for Composites (ASC) 36th Annual Technical VIRTUAL Conference, College Station, TX, USA, 20–22 September 2021; pp. 1178–1190.
14. Smeets, E.T.B.; Rans, C.D.; Castro, S.G.P.; Villegas, I.F. To measure is to know: Evaluating indirect measurement techniques for observing the damage tolerance behaviour of spot welded thermoplastic composites. *J. Adv. Join. Process.* **2023**, *8*, 100152. [CrossRef]
15. Travieso-Puente, R.; Martín-Pérez, C.; González-Castro, N.; Rodríguez-Senín, E.; Vidal-Navarro, J.; Vicente-Guerrero, G.; Veldman, S. ECO-CLIP: Circular economy from factory waste material towards aircraft structural components. *IOP Conf. Ser. Mater. Sci. Eng.* **2022**, *1226*, 012104. [CrossRef]
16. One of the World's Largest Thermoplastic Aerostructures Successfully Completed in Stunning Project. Available online: https://www.gknaerospace.com/news-insights/news/one-of-the-worlds-largest-thermoplastic-aerostructures-successfully-completed-in-stunning-project/ (accessed on 1 September 2024).
17. Brito, C.B.G.; Teuwen, J.; Dransfeld, C.A.; Villegas, I.F. On improving process efficiency and weld quality in ultrasonic welding of misaligned thermoplastic composite adherends. *Compos. Struct.* **2023**, *304*, 116342. [CrossRef]